



## Lean and ultralean stretched propane–air counterflow flames

Zhongxian Cheng<sup>a</sup>, Robert W. Pitz<sup>a,\*</sup>, Joseph A. Wehrmeyer<sup>b</sup>

<sup>a</sup> Mechanical Engineering Department, Vanderbilt University, Box 1592, Station B, Nashville, TN 37235, USA

<sup>b</sup> Aerospace Testing Alliance, Building 1099, Avenue C, Arnold Air Force Base, TN 37389, USA

Received 19 April 2005; received in revised form 9 February 2006; accepted 21 February 2006

Available online 24 March 2006

### Abstract

Stretched laminar flame structures for a wide range of C<sub>3</sub>H<sub>8</sub>–air mixtures vs hot products are investigated by laser-based diagnostics and numerical simulation. The hot products are produced by a lean H<sub>2</sub>–air premixed flame. The effect of stretch rate and equivalence ratio on four groups of C<sub>3</sub>H<sub>8</sub>–air flame structures is studied in detail by Raman scattering measurements and by numerical calculations of the major species concentration and temperature profiles. The equivalence ratio,  $\phi$ , is varied from a near-stoichiometric condition ( $\phi = 0.86$ ) to the sublean limit ( $\phi = 0.44$ ) and the stretch rate varies from 90 s<sup>-1</sup> to near extinction. For most of these C<sub>3</sub>H<sub>8</sub>–air lean mixtures, hot products are needed to maintain the flame. The significant feature of these flames is the relatively low flame temperatures (1200–1800 K). For this temperature range, the predicted C<sub>3</sub>H<sub>8</sub>–air flame structure is sensitive to the specific chemical kinetic mechanism. Two types of flame structures (a lean self-propagating flame and a lean diffusion-controlled flame) are obtained based on the combined effect of stretch and equivalence ratio. Three different mechanisms, the M5 mechanism, the Optimized mechanism, and the San Diego mechanism, are chosen for the numerical simulations. None of the propane chemical mechanisms give good agreement with the data over the entire range of flame conditions.

© 2006 The Combustion Institute. Published by Elsevier Inc. All rights reserved.

**Keywords:** Raman scattering; Propane; Planar; Counterflow; Opposed jet

### 1. Introduction

Lean premixed combustion provides clean and efficient burning in practical devices, such as direct injection spark ignition engines and lean-burn gas turbine engines. Lean premixed flames in these devices are turbulent and unsteady. To understand the effect of high stretch rate (flame stretch) in these de-

vices, planar opposed jet premixed flames have been investigated. An opposed-jet burner generates counterflow flames that are widely used to study chemical kinetics and molecular species transport under aerodynamic stretch [1,2]. In particular, opposed partially premixed CH<sub>4</sub>–air flame structures vs air were investigated [3–5]. Lean partially premixed methane–air and propane–air flame structures vs hot products have also been investigated [6–9].

For lean-limit premixed reactants opposed by hot products, analytical and numerical studies indicate that the reaction surface moves toward the stagnation

\* Corresponding author. Fax: +1 615 343 6687.  
E-mail address: [robert.w.pitz@vanderbilt.edu](mailto:robert.w.pitz@vanderbilt.edu)  
(R.W. Pitz).

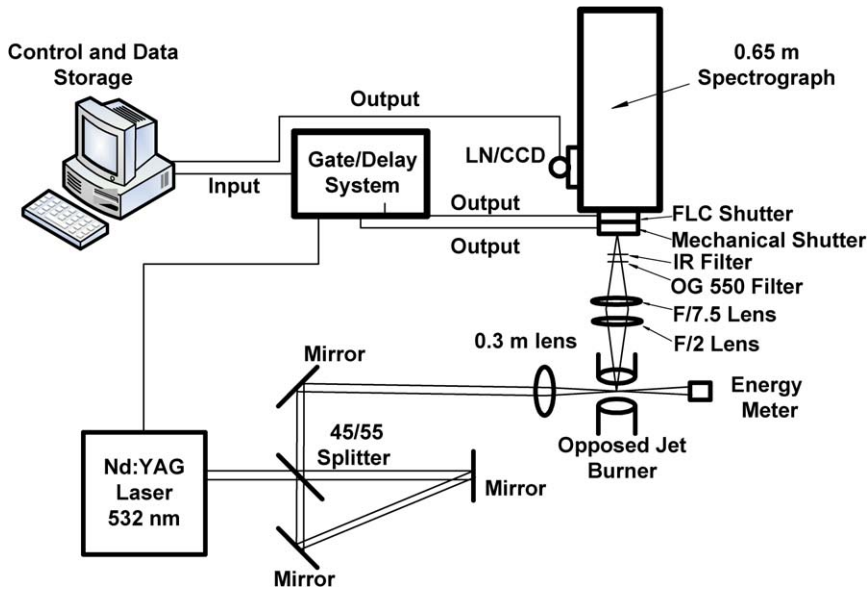


Fig. 1. Schematic of the Raman system.

plane and locates on the hot products side of the stagnation point when increasing the stretch rate [10–15]. Pollutants can be formed in very lean regions of direct injection engines, but the presence of hot products can improve combustion in these regions. In an effort to understand how the presence of hot products influences lean combustion, a set of  $C_3H_8$ –air flames with a wide range of equivalence ratios and stretch rates impinging upon hot products are studied experimentally and numerically. The concept of “negative flame speed” was put forward by Williams [16] and Sohrab et al. [17] based on the experimental investigation of two counterflow premixed methane–air flames. In this work, negative flame speed propane–air flame structures are studied with an opposed-jet burner. The present work extends the previous efforts [6,8] by investigating a wider range of experimental conditions. The stretch effects on the flame structure of the interaction between hot products and lean  $C_3H_8$ –air mixtures are studied by experiment and simulation. The hot products are produced by a lean  $H_2$ –air flame ( $\phi = 0.28$ ). Several chemical kinetic reaction mechanisms are used to perform the simulation and the comparisons among the kinetic mechanisms are discussed.

## 2. Experimental system and flames examined

Measurements of major species concentrations and temperature are made along the centerline of an opposed-jet burner using the laser Raman scattering technique. A schematic of the visible Raman system

is shown in Fig. 1. A 532-nm Nd:YAG laser beam (200 mJ/pulse) is temporally stretched from 7 to 35 ns with a beam splitter/mirror system and focused by a 0.3-m lens. A Stanford Research Systems DG535 pulse generator synchronizes the trigger signals in the system. The Raman light collecting system in [6] is modified by replacing the F/1.5 Cassegrain with a 75-mm-diameter F/2 lens. The collimated light from this F/2 lens is focused by a 75-mm-diameter F/7.5 lens, passed through a ferroelectric shutter, a mechanical shutter, and an entrance slit to the 0.65-m spectrometer (SPEX 1800, 0.75-m Czerny Tuner Spectrometer, modified to 0.65 m). A mechanical shutter (Uniblitz) is used as an external shutter for the liquid nitrogen-cooled CCD camera but has a relatively long exposure time (6 ms). A ferroelectric liquid crystal shutter is heated (38 °C) to obtain a short exposure time (30  $\mu$ s) and placed in front of the mechanical shutter to cut off flame luminosity into the spectrometer. A Schott orange glass filter is placed in front of the entrance slit to block any stray 532-nm light. A separate filter (dielectric short wave pass filter, 750-nm cutoff) is mounted at the entrance slit to eliminate the infrared radiation from the flame.

A liquid-nitrogen-cooled, charge-coupled device (LN/CCD) is used to obtain the Raman spectra. The LN/CCD camera has a  $1024 \times 1024$  pixel chip ( $24 \times 24 \mu\text{m}/\text{pixel}$ ), mounted to the back plane of the spectrometer. The chip is back-illuminated to give high quantum efficiency in the visible. Planar flames generated by a round opposed-jet burner are studied. The laser beam is parallel to the flame and is perpendicular to the concentration gradient axis. The measuring

Table 1  
Flame parameters

Group	C <sub>3</sub> H <sub>8</sub> –air, $\phi$	H <sub>2</sub> –air, $\phi$	Stretch rate, $\kappa$ (s <sup>-1</sup> )
A	0.75	0.28	90
			140
			252
B	0.66	0.28	90
			140
			252
C	0.44	0.28	140
	0.55		140
D	0.75	0	140
	0.86	0.28	140
	0.86	0	140

sample volume is a cylinder (length is 4.7 mm and diameter is 0.2 mm). For a planar flame measurement, the 0.2-mm dimension is transverse to the concentration gradient. Thus, the 0.2-mm dimension is the spatial resolution of the system. The sample volume length is limited by the entrance slit image and is about 4.7 mm. The planar flame composition does not vary along the 4.7-mm beam length and hence the 640 pixels along the spatial dimensions are binned into one super pixel.

The opposed-jet burner used for this work was modified from the design by Seshadri and co-workers [18]. It consists of two 25-mm-diameter straight jets, which are separated by 12.6 mm. The nozzle exits are further modified for this work. Honeycomb inserts replace the screens used previously [6,7] and are placed flush with the tube exits to give very uniform jet exit velocity profiles.

Table 1 lists the flame parameters studied in this work. Four groups of flames classified by equivalence ratio are studied. The global stretch rate

$$\kappa = \frac{2V_O}{L} \left( 1 + \frac{V_F \sqrt{\rho_F}}{V_O \sqrt{\rho_O}} \right)$$

for the planar opposed-jet flame, as defined by Kim et al. [19], is used here, where  $L$  is the separation distance between the two jets ( $L = 12.6$  mm for the current study) and  $V$  and  $\rho$  are velocity and density of inlet gas streams, respectively. The subscript O indicates the hydrogen–air stream, and subscript F indicates the hydrocarbon–air stream. Group A includes three propane–air mixtures (which have a 0.75 equivalence ratio) vs a lean hydrogen–air mixture at stretch rates of 90, 140, and 252 s<sup>-1</sup>. Group B includes three propane–air mixtures, which have a 0.66 equivalence ratio vs a lean hydrogen–air mixture at stretch rates of 90, 140, and 252 s<sup>-1</sup>. Group C includes an ultralean sublimit propane–air mixture or a near-limit propane–air mixture (equivalence ratio of 0.44 or 0.55) vs a

lean hydrogen–air mixture at a stretch rate of 140 s<sup>-1</sup>. Group D includes several stronger self-propagating flames. They are formed by propane–air mixtures which have equivalence ratios of 0.75 or 0.86 vs air or a hydrogen–air mixture at a global stretch rate of 140 s<sup>-1</sup>. All of the lean hydrogen–air mixtures have the same equivalence ratio of 0.28. Fig. 2 shows a set of Raman spectral graphs from the premixed opposed-jet flame: C<sub>3</sub>H<sub>8</sub>–air ( $\phi = 0.75$ ) vs H<sub>2</sub>–air ( $\phi = 0.28$ ). The spectrum at each position is a composite of the CCD spectral images taken at two diffraction grating positions. There are three representative spectra for three different locations along the centerline of the opposed-jet burner. Each spectrum is the result of a 100 shots accumulation of light signals onto the CCD, and each spectrum has background luminosity subtracted. The strong C–H stretch Raman line at 629 nm (2900 cm<sup>-1</sup> shift) is used to measure the propane fuel concentration. As a result, all hydrocarbon species (C<sub>1</sub>–C<sub>3</sub>) that exhibit a C–H stretch vibration are reflected in the propane measurement. It is found that all laser-induced background levels are much lower than the previous results [6] due to improvements in the detection system.

### 3. Simulation and kinetic mechanisms

Numerical predictions are obtained from the OPPDIF program of the CHEMKIN Collection [20]. Detailed chemical kinetic mechanisms and transport data (mixture-average formulation) are used for numerical predictions. The M5 propane mechanism by Haworth et al. [21], the San Diego mechanism [22], and an Optimized mechanism of C<sub>1</sub>–C<sub>3</sub> combustion mechanism by Qin et al. [23] are employed for the numerical simulations of propane–air flames. Table 2 lists the number of species and the number of reactions for the three chemical kinetic mechanisms. The flames in this work have relatively high strain rates (short residence times) and relatively low temperatures (lean conditions with maximum temperatures of ~1800 K or less). Also, the flames appear blue in the experiment without any apparent soot emission. Thus gas radiation and soot radiation are not included in the simulations.

## 4. Results and discussion

### 4.1. Group A: Stretched propane–air flames with $\phi = 0.75$ vs hot products

All flames shown in this subsection have the equivalence ratio ( $\phi = 0.75$ ). They are propane–air ( $\phi = 0.75$ ) vs hydrogen–air ( $\phi = 0.28$ ). It is known

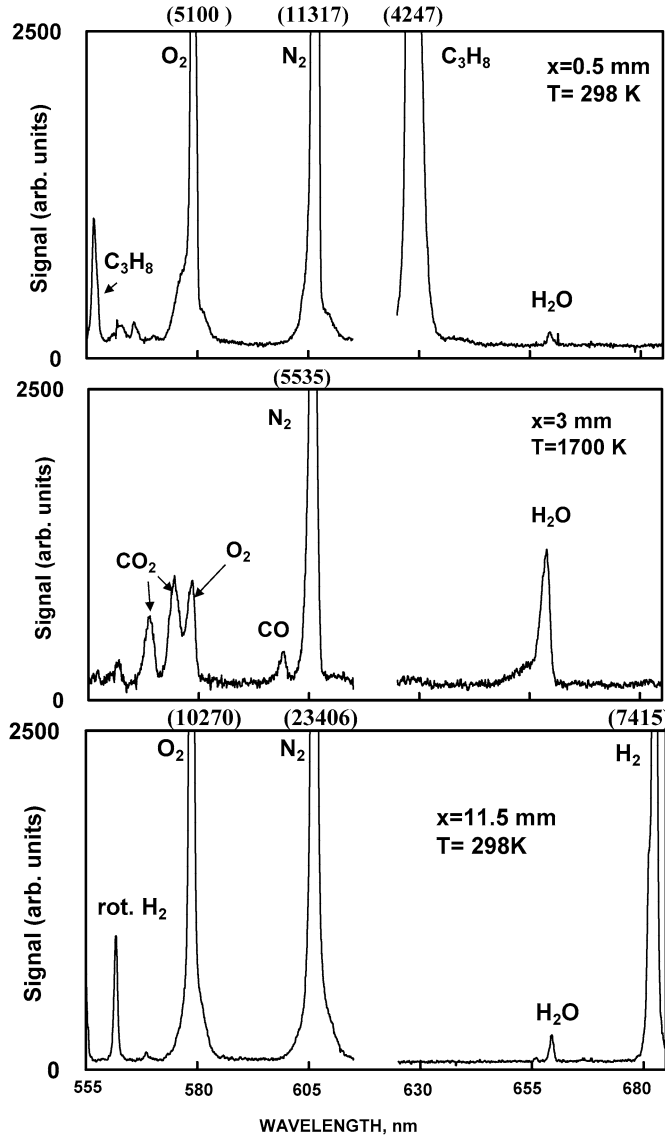


Fig. 2. Representative Raman spectra obtained from the flame ( $\text{C}_3\text{H}_8$ -air,  $\phi = 0.75$  vs  $\text{H}_2$ -air,  $\phi = 0.28$  at  $\kappa = 140 \text{ s}^{-1}$ ) shown in Fig. 5. Spectra correspond to three axial positions along the centerline of the opposed-jet burner where  $x$  is the distance from the top jet.

Table 2  
Propane-air chemical kinetic mechanisms

Mechanisms	Number of species	Number of reactions
San Diego	39	179
Optimized	70	463
M5	28	73

that this kind of propane-air flame is above the lean flammability limit ( $\phi = 0.56$ ) [24]. The equivalence ratios for the two streams are fixed and the aerodynamic stretch rate varies from a relatively low  $90 \text{ s}^{-1}$

to near the extinction limit  $252 \text{ s}^{-1}$ . When the stretch rate is below some level (i.e.,  $140 \text{ s}^{-1}$ ), the flames are premixed and relatively strong (Figs. 3–6). Near the extinction condition ( $\kappa = 252 \text{ s}^{-1}$ ), the flame becomes very weak, even though the equivalence ratio is still 0.75. It is impossible to form a premixed flame and the relevant flame structure is given in Fig. 7.

Experimental measurements and numerical predictions of temperature and reactant concentrations are compared in Fig. 3 for the propane-air ( $\phi = 0.75$ ) mixture vs hot products at stretch rate  $\kappa = 90 \text{ s}^{-1}$ . As seen from the experimental data, a premixed “pos-

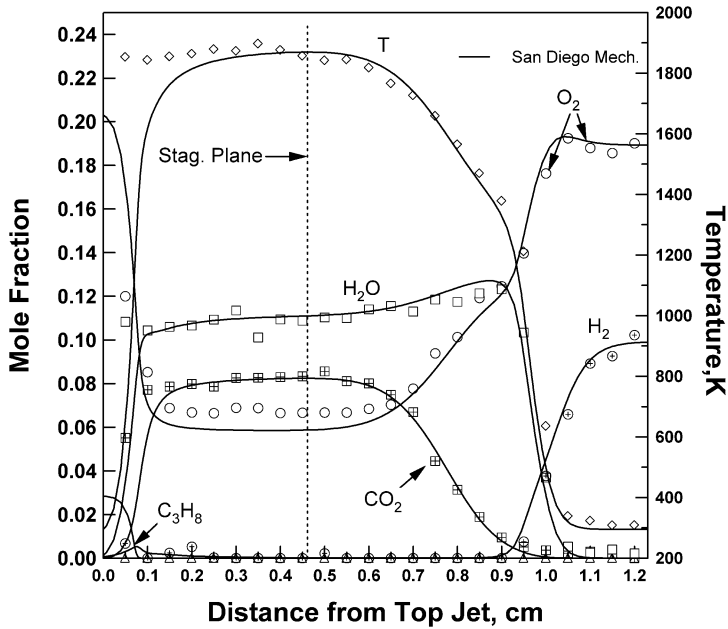


Fig. 3. Experimental and numerically predicted species and temperature profiles for a premixed opposed-jet flame:  $C_3H_8$ -air ( $\phi = 0.75$ ) vs  $H_2$ -air ( $\phi = 0.28$ ),  $\kappa = 90 \text{ s}^{-1}$ . Numerical simulation using the San Diego mechanism.

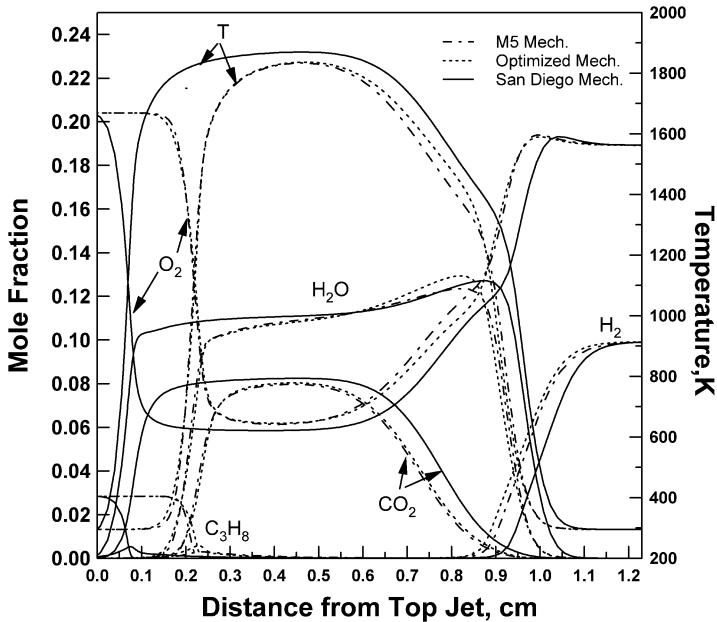


Fig. 4. Comparison of numerically predicted species and temperature profiles for a premixed opposed-jet flame:  $C_3H_8$ -air ( $\phi = 0.75$ ) vs  $H_2$ -air ( $\phi = 0.28$ ),  $\kappa = 90 \text{ s}^{-1}$  with three different mechanisms.

itive flame speed” flame exists on the propane-air side of the stagnation plane. Numerical predictions are performed using three different chemical kinetic mechanisms (M5, San Diego, and Optimized mechanisms). The results shown in Fig. 3 are from the San Diego mechanism. At this stretch rate and stoichiom-

etry, the propane-air flame is so close to the exit of the jet that the starting point of the flame cannot be distinguished in the experimental data. Near the exit of the jet, the experimental data for temperature, oxygen, and fuel species concentrations differ from the predicted results using the San Diego mechanism. At

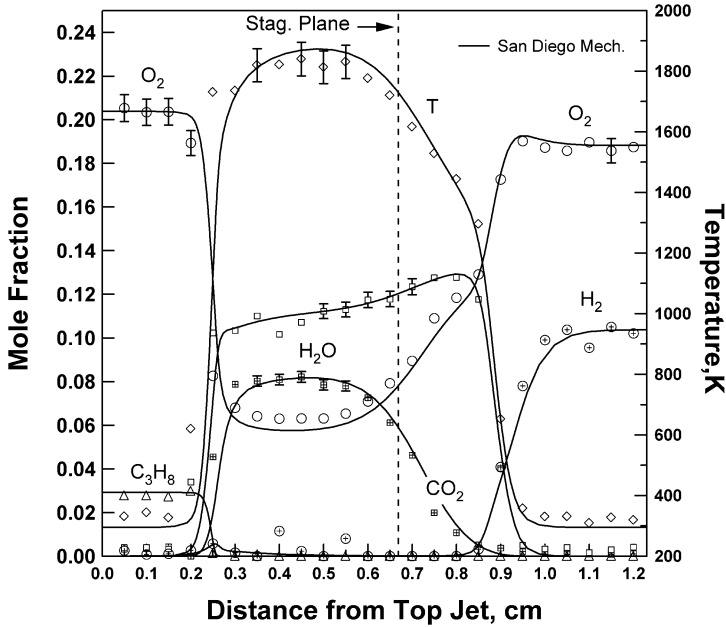


Fig. 5. Experimental and numerically predicted species and temperature profiles for a premixed opposed-jet flame:  $C_3H_8$ -air ( $\phi = 0.75$ ) vs  $H_2$ -air ( $\phi = 0.28$ ),  $\kappa = 140 \text{ s}^{-1}$ . Numerical simulation using the San Diego mechanism.

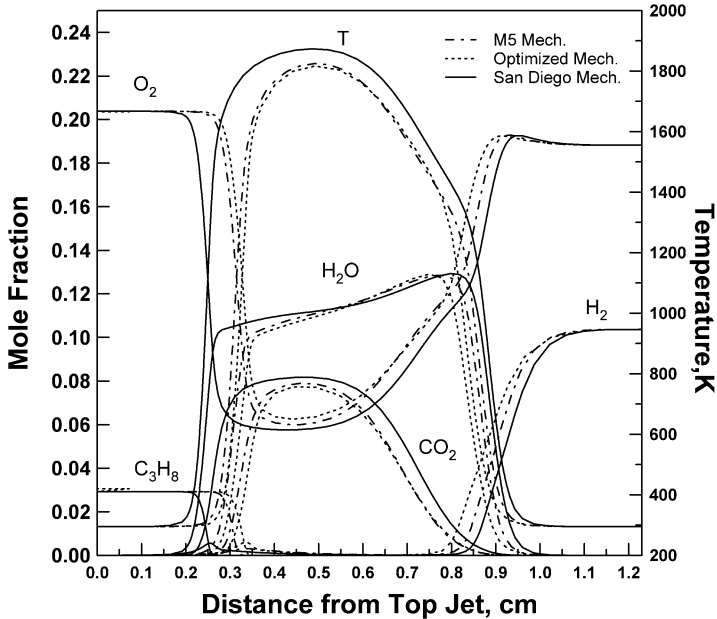


Fig. 6. Comparison of numerically predicted species and temperature profiles for a premixed opposed-jet flame:  $C_3H_8$ -air ( $\phi = 0.75$ ) vs  $H_2$ -air ( $\phi = 0.28$ ),  $\kappa = 140 \text{ s}^{-1}$  with three different mechanisms.

the premixed propane-air flame zone, the temperature profile from the experiment is higher than the predicted results. From the propane-air flame zone to the  $H_2$ -air side, the oxygen, carbon dioxide, and water vapor have very good agreement with the predictions.

The comparisons based on the numerical simulations using three different mechanisms are shown in Fig. 4. From Fig. 4, it is seen that there are some deviations for the predictions using the three mechanisms. The most obvious deviation is the propane-air flame location. The prediction of the flame location

Table 3  
Summary of the modeling using three chemical kinetic mechanisms

Group	C <sub>3</sub> H <sub>8</sub> /air $\phi$	H <sub>2</sub> /air $\phi$	$\kappa$ (s <sup>-1</sup> )	Exp.	San Diego		Optimized		M5	
						S <sub>L</sub> <sup>d</sup> (cm/s)		S <sub>L</sub> <sup>d</sup> (cm/s)		S <sub>L</sub> <sup>d</sup> (cm/s)
A	0.75	0.28	90	+ <sup>a</sup>	+	20.47	+	18.58	+	18.77
			140	+	+	23.75	+	22.17	+	23.21
			252	- <sup>b</sup>	+	28.61	-	n/a		ext. <sup>c</sup>
B	0.66	0.28	90	+	+	19.22	+	18.16	+	18.61
			140	-	+	26.09	-	n/a	-	n/a
			252	-	-	n/a	-	n/a		ext.
C	0.44	0.28	140	-	-	n/a		ext.	-	n/a
	0.55		140	-	-	n/a	-	n/a	-	n/a
D	0.75	0	140	+	+	33.35	+	24.69	+	24.90
	0.86	0.28	140	+	+	39.14	+	36.03	+	36.04
	0.86	0	140	+	+	36.41	+	32.18	+	32.64

<sup>a</sup> + sign means “positive flame speed” flame.

<sup>b</sup> - sign means “negative flame speed” flame.

<sup>c</sup> ext. means extinction.

<sup>d</sup> Propane–air flame speed.

with the San Diego mechanism may be compromised by thermal diffusion into the inlet. The predictions using the M5 and the Optimized mechanisms give very similar results. Analysis of Figs. 3 and 4 implies that the San Diego mechanism gives better agreement than the other two mechanisms. Also it indicates that the San Diego mechanism predicts a higher laminar flame speed which has been noted earlier in Ref. [8].

Experimental measurements and numerical predictions of temperature and reactant concentrations are compared in Fig. 5 for the propane–air ( $\phi = 0.75$ ) mixture vs hot products at a stretch rate of 140 s<sup>-1</sup>. Overall uncertainty is estimated to be about 3% based on the measurements in the Hencken calibration burner. The representative error bars are shown in Fig. 5. As seen from the experimental data, a premixed positive flame speed flame exists on the propane–air side of the stagnation plane. The results shown in Fig. 5 are from the San Diego mechanism. It is found that the premixed propane–air flame locates at 2.5 mm and the lean hydrogen–air flame locates at 9 mm from the propane jet exit. The temperature profile implies that the two flames are far away from each other. The flame location is determined by the balance between the reactant velocity and the laminar flame speed. At the higher stretch rate of 140 s<sup>-1</sup>, the flame moves toward the stagnation plane (Fig. 5). The predicted propane–air flame location slightly differs from the actual location while the hydrogen–air flame location is well predicted.

Experimental data for temperature is slightly lower than predicted. Carbon dioxide and water va-

por from the experiment have very good agreement with predicted results. On the hydrogen–air flame side, there is very good agreement. The comparison using different mechanisms is shown in Fig. 6. Compared to the flame structure shown in Fig. 4 for the case of  $\kappa = 90$  s<sup>-1</sup>, the discrepancies between the three mechanisms are becoming smaller with increased stretch rate. From Figs. 5 and 6, it is seen that the predictions using the M5 and Optimized mechanisms do not match the data as well as the San Diego mechanism. The most obvious deviation is the propane–air flame location that is caused by different propane–air flame propagation speeds for the various chemical kinetic mechanisms. The propane–air flame speeds from the simulations are listed in Table 3 for the different flame conditions and chemical kinetic mechanisms. In contrast, measured and calculated flame temperature and species concentration agree very well on the hydrogen–air flame side, particularly for the San Diego mechanism. From Fig. 6, it is indicated that the San Diego mechanism predicts a higher laminar flame speed for both hydrogen–air and propane–air flames. The results from the M5 mechanism and the Optimized mechanism are almost identical at this stretch rate.

Keeping everything unchanged except stretch rate, the flame structure near the extinction condition ( $\kappa = 252$  s<sup>-1</sup>) is given in Fig. 7. The experimental data show a very weak propane diffusion flame merged with the lean hydrogen–air premixed flame. A small amount of propane diffuses across the stagnation flame to burn in the lean premixed hydrogen–air flame. The peak temperature is around 1400 K. The

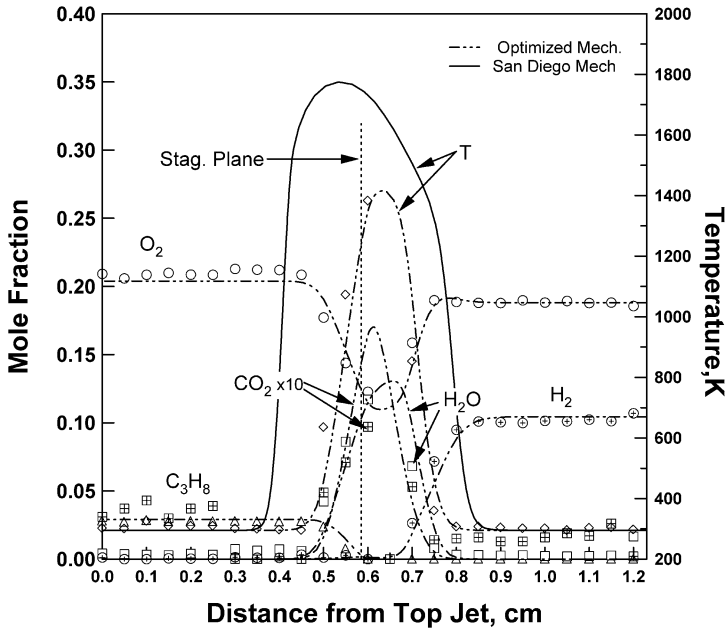


Fig. 7. Experimental and numerically predicted species and temperature profiles for a premixed opposed-jet flame:  $C_3H_8$ –air ( $\phi = 0.75$ ) vs  $H_2$ –air ( $\phi = 0.28$ ),  $\kappa = 252 \text{ s}^{-1}$ . Numerical simulation using the Optimized mechanism. The predicted temperature profile from the San Diego mechanism is also shown in the figure for comparison. The M5 mechanism predicts extinction.

experimental data agree very well with predicted results from the Optimized mechanism, but the data strongly deviate from the predictions by the M5 mechanism (not shown in Fig. 7) or the San Diego mechanism (only the temperature profile is shown in Fig. 7). The numerical results with the San Diego mechanism indicate a stronger premixed flame at this situation (temperature is about 1800 K); on the other hand, results from the M5 mechanism indicate that extinction has already occurred. Fewer reactions are included in the M5 mechanism (see Table 2) and it may not be appropriate for this high stretch rate case as discussed later. The San Diego mechanism was developed for flames and high-temperature ignition and in general gives higher flame speeds (see Table 3). For the San Diego mechanism, the higher predicted flame speed delays the transition from a self-propagating premixed propane–air flame to a weak propane diffusion flame to a higher stretch rate ( $\kappa > 252 \text{ s}^{-1}$ ). This transition to the weak diffusion flame is very sensitive to the flame speed at high stretch rate and hence is very sensitive to the specific chemical kinetic mechanism.

The thermal diffusivity coefficient of a lean propane–air mixture is  $0.208 \text{ cm}^2/\text{s}$  and the mass diffusivity of deficient reactant (propane diffusing in air) is  $0.114 \text{ cm}^2/\text{s}$  [25]. Thus, Lewis number,  $Le$ , which is the ratio of thermal diffusivity to mass diffusivity, is 1.82 and is greater than unity producing preferen-

tial diffusion. According to Law [1] and Sung et al. [26], the combination of stretch rate and Lewis number effect should cause the flame temperature to decrease with stretch rate for  $Le > 1$ . This is confirmed by the slight decrease in the measured temperature from  $\kappa = 90 \text{ s}^{-1}$  ( $T_{\max} = 1896 \text{ K}$ ) to  $\kappa = 140 \text{ s}^{-1}$  ( $T_{\max} = 1840 \text{ K}$ ).

The effect of nonunity Lewis number on the structure of the lean propane–air vs lean hydrogen–air flame is also seen by the effect of stretch on absolute temperature gradients. As seen in Fig. 8, with increasing stretch rate from 90 to  $140 \text{ s}^{-1}$ , the temperature gradient decreases on the propane–air flame side. This is because the lean propane–air mixture has a Lewis number much greater than unity, and the stretch rate weakens the flames. When the stretch rate increases up to  $252 \text{ s}^{-1}$  and the flame turns into a diffusion-controlled negative flame speed [17] flame, the temperature gradient decreases further. On the other hand, the Lewis number for hydrogen–air is much less than unity and hydrogen has strong preferential diffusion that strengthens the flame. In this situation, stretch rate can increase the temperature gradient. The trend of the effect of stretch on temperature gradient is exactly opposite that of the propane–air flame. In addition, the thermal-diffusion effect (Soret effect) on the flame temperature profiles has been calculated (not shown). It is found that the Soret effect is very small and is negligible.

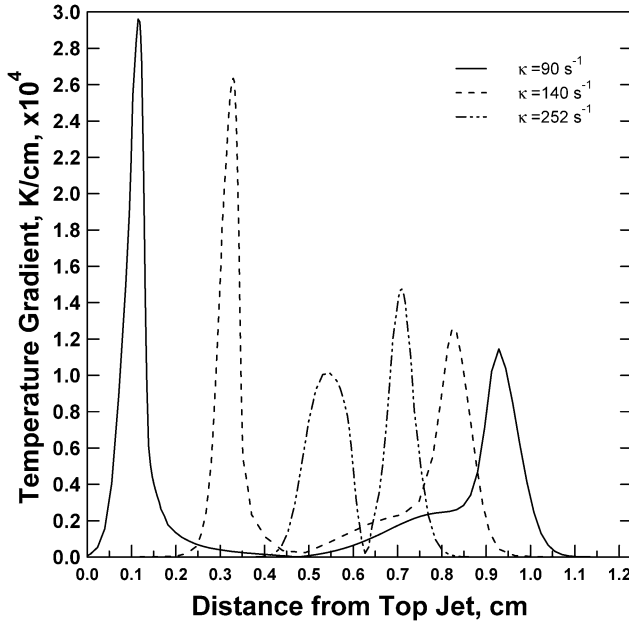


Fig. 8. Numerically predicted temperature gradient at different stretch rates for  $\text{C}_3\text{H}_8$ -air ( $\phi = 0.75$ ) vs  $\text{H}_2$ -air ( $\phi = 0.28$ ),  $\kappa = 90, 140,$  and  $252 \text{ s}^{-1}$ . Temperature gradients are from the Optimized mechanism.

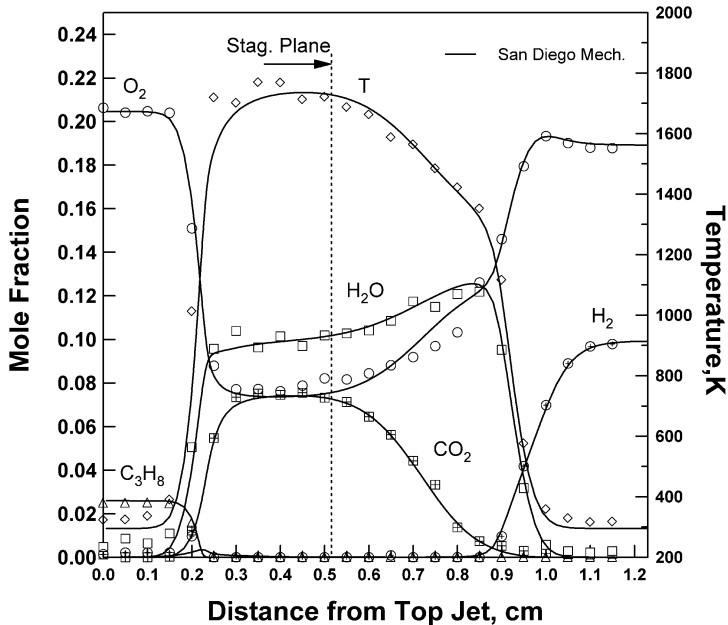


Fig. 9. Experimental and numerically predicted species and temperature profiles for a premixed opposed-jet flame:  $\text{C}_3\text{H}_8$ -air ( $\phi = 0.66$ ) vs  $\text{H}_2$ -air ( $\phi = 0.28$ ),  $\kappa = 90 \text{ s}^{-1}$ . Numerical simulation using the San Diego mechanism.

#### 4.2. Group B: Stretched propane-air flames with $\phi = 0.66$ vs hot products

All flames shown in this subsection have the same equivalence ratio: propane-air ( $\phi = 0.66$ ) vs hydrogen-air ( $\phi = 0.28$ ). Again, the aerodynamic

stretch rate varies from  $90 \text{ s}^{-1}$  to near extinction  $252 \text{ s}^{-1}$ . Compared to Group A, the propane-air flames of Group B have slightly leaner mixtures. At  $\kappa = 90 \text{ s}^{-1}$ , the flame structure shown in Fig. 9 is similar to the structure shown in Fig. 3 for  $\phi = 0.75$ . The only difference is that the propane-air flame moves

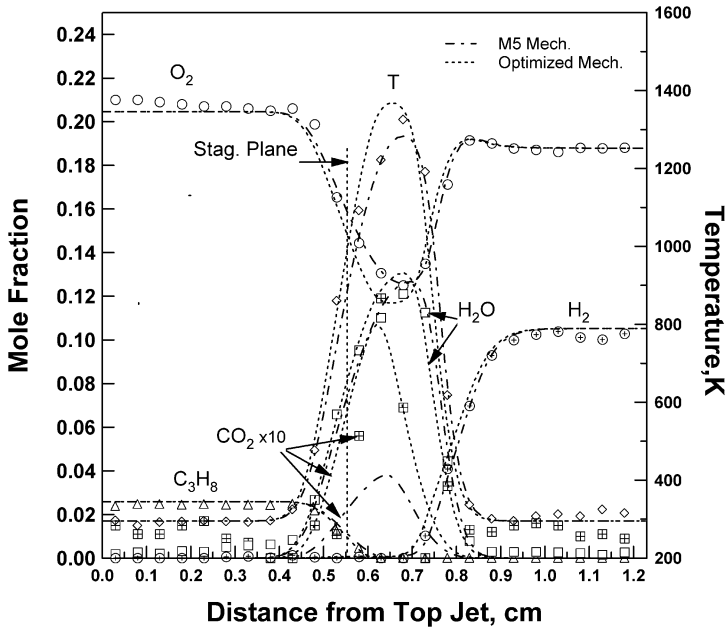


Fig. 10. Experimental and numerically predicted species and temperature profiles for a premixed opposed-jet flame:  $C_3H_8$ –air ( $\phi = 0.66$ ) vs  $H_2$ –air ( $\phi = 0.28$ ),  $\kappa = 140 \text{ s}^{-1}$ . Numerical simulation using the M5 mechanism and the Optimized mechanism.

toward the stagnation plane. This is because the flame speed decreases, even though the stretch rate is unchanged. In addition, comparisons of numerical simulations using three different mechanisms still indicate that the San Diego mechanism predicts the highest flame speed of the various mechanisms (see Table 3) and gives the best overall prediction of the data. When increasing stretch rate to  $\kappa = 140 \text{ s}^{-1}$ , the lean premixed propane–air mixture diffuses across the stagnation plane to form a weak diffusion flame (Fig. 10), since the stagnation plane is diffusionally “penetrable.” The numerical simulations in Fig. 10 come from the Optimized mechanism and the M5 mechanism. Comparing data with predictions indicates that the temperature and most of the species concentrations agree well except carbon dioxide. The experimental carbon dioxide data agree with the Optimized mechanism predictions better than the M5 mechanism predictions. These results are consistent with previous work by Wehrmeyer et al. [6] that shows that the M5 mechanism gives a carbon dioxide prediction one order of magnitude lower than the experimental value for a negative flame speed flame. When this flame is modeled using the San Diego mechanism, the flame structure is different and it is shown in Fig. 11. The prediction of the stagnation plane (indicated by the dashed line) comes from the simulation using the Optimized mechanism. Obviously, the predictions using the San Diego mechanism are far away from the experimental data. The San Diego mechanism was developed for high-temperature flames and predicts

higher propane–air flame speeds than the other mechanisms (see Table 3). The higher flame speed delays the transition from a self-propagating premixed flame to a weak diffusion flame and leads to its poor prediction of the weak diffusion flame in Fig. 10.

Fig. 12 shows the flame structure for a stretch rate  $\kappa = 252 \text{ s}^{-1}$ . The flame itself is very similar to  $\kappa = 140 \text{ s}^{-1}$ , except the reaction zone is narrower. Usually for a diffusion flame, the flame thickness scales inversely with  $\kappa^{1/2}$ . Here it is not a pure diffusion flame, but a negative flame speed propane–air diffusion flame supported by a lean premixed hydrogen–air flame. But the trend is still true for this case; that is, the flame reaction zone is becoming narrower when increasing stretch rate. Similarly, incomplete reaction caused by higher stretch rate eventually leads to extinction even though hot products from the lean hydrogen–air flame can extend this extinction up to much higher stretch rates. Both the San Diego and Optimized mechanisms give a good prediction of this low temperature flame. Since the stretch rate is very high and well above the sensitive transition from a self-propagating premixed flame to a weak merged flame, the San Diego mechanism does well here. The M5 mechanism predicts extinction for this case. The M5 mechanism is a shortened and modified version of the Warnatz alkane combustion mechanism [27]. It was created to be efficient in direct numerical simulations (DNS) of turbulent combustion. The M5 mechanism predicts propane–air flame speeds that are only slightly higher than the

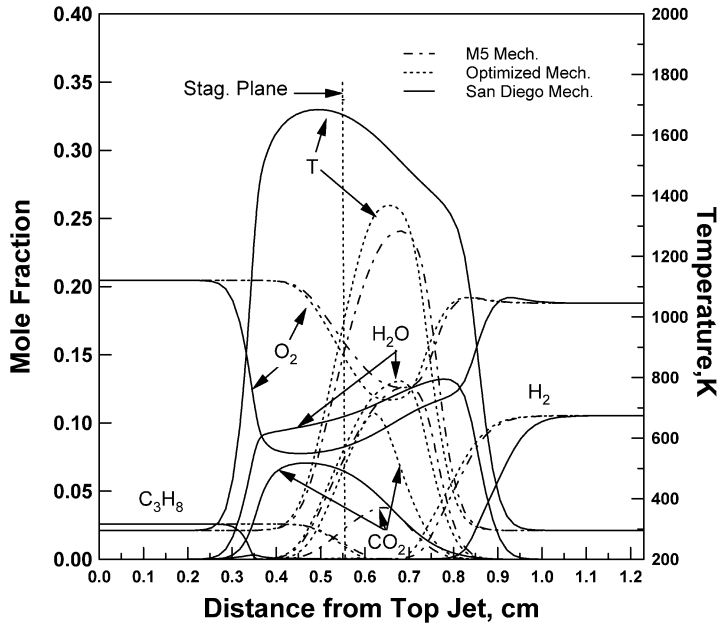


Fig. 11. Comparison of numerically predicted species and temperature profiles with three different mechanisms for a premixed opposed-jet flame:  $C_3H_8$ -air ( $\phi = 0.66$ ) vs  $H_2$ -air ( $\phi = 0.28$ ),  $\kappa = 140 \text{ s}^{-1}$ .

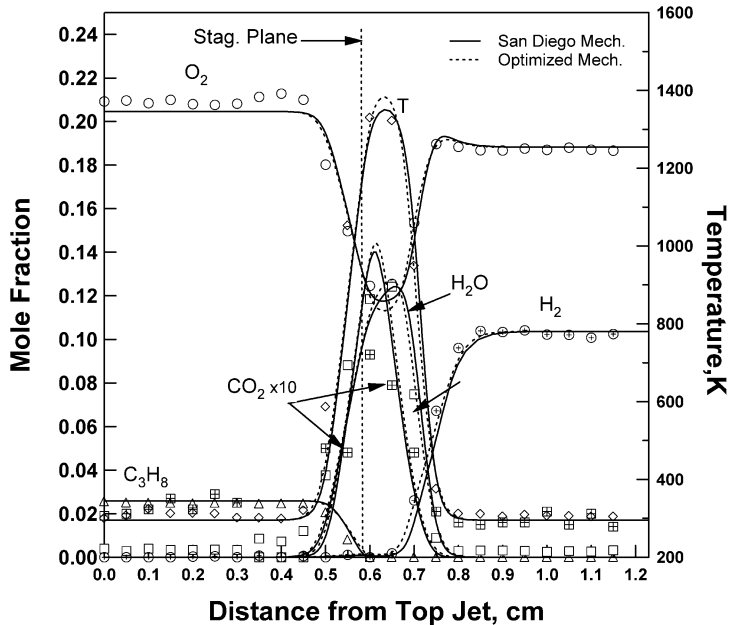


Fig. 12. Experimental and numerically predicted species and temperature profiles for a premixed opposed-jet flame:  $C_3H_8$ -air ( $\phi = 0.66$ ) vs  $H_2$ -air ( $\phi = 0.28$ ),  $\kappa = 252 \text{ s}^{-1}$ . Numerical simulation using the San Diego mechanism and the Optimized mechanism. The M5 mechanism predicts extinction.

original Warnatz mechanism [21]. To create the M5 mechanism that is efficient in DNS, the computational stiffness was reduced by eliminating reactions with short chemical time scales from the original Warnatz mechanism. For example, some fuel breakdown steps

were made irreversible and  $n$ - $C_3H_7$  that forms in a short time-scale reaction was eliminated [21]. This could explain its inaccuracy near extinction conditions where these short chemical time-scale reactions are important.

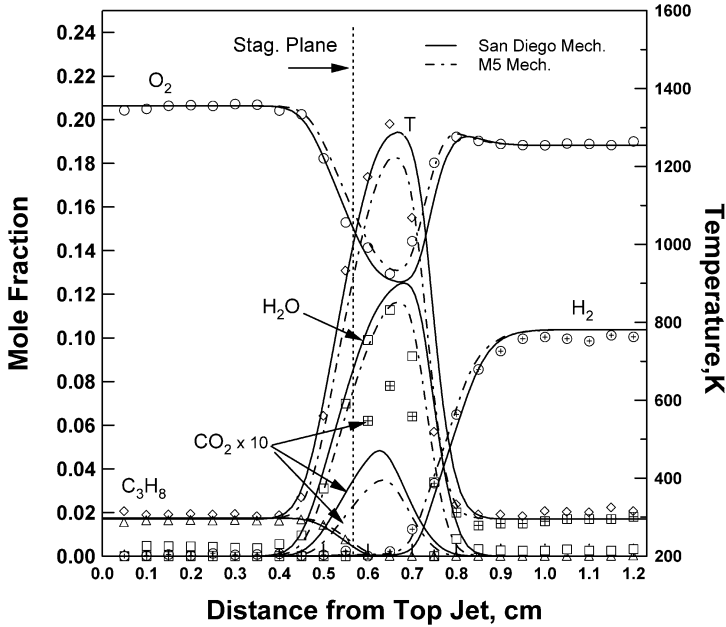


Fig. 13. Experimental and numerically predicted species and temperature profiles for a premixed opposed-jet flame:  $C_3H_8$ –air ( $\phi = 0.44$ ) vs  $H_2$ –air ( $\phi = 0.28$ ),  $\kappa = 140 \text{ s}^{-1}$ . Numerical simulation using the San Diego mechanism and the M5 mechanism. The Optimized mechanism predicts extinction.

#### 4.3. Group C: Stretched sublimit propane–air flames

It is known that the lean limit for propane–air mixture is 5% (fuel by volume) or  $\phi = 0.56$ . Based on the definition of flammability limit, a mixture will be impossible to burn at any condition if it is under the lean limit. But, Ju et al. [28,29] numerically studied sublimit combustion at very low stretch rate and found that sublimit flames exist, particularly for premixed flames with deficient-reactant Lewis numbers less than one where moderate stretch strengthens the flame. In this work, the deficient-reactant Lewis number is greater than one (1.82) and moderate stretch will weaken the flame. However, the lean limit of the propane–air flame can be extended if the mixture interacts with the hydrogen–air flame, even though the flame is very weak.

Fig. 13 shows the sublimit flame structure of  $C_3H_8$ –air mixture ( $\phi = 0.44$ ) vs  $H_2$ –air ( $\phi = 0.28$ ) mixture ( $\kappa = 140 \text{ s}^{-1}$ ). This is a very weak negative flame speed flame. The flame temperature drops to 1300 K. Since the ultralean propane–air mixture is beyond the flammability limit, there will be no transition from a self-propagating premixed propane–air flame to a weak diffusion flame and the differences in the propane–air flame speeds shown in Table 3 are not important. Under these sublimit conditions, only the weak diffusion flame is formed. Predictions based on the San Diego mechanism give good agree-

ment with experimental data for temperature and most reactants except carbon dioxide. The measured carbon dioxide is higher than predicted with both the San Diego mechanism and the M5 mechanism. The San Diego mechanism works well for the ultra-weak flame, the M5 mechanism predicts a slightly weaker flame, but the Optimized mechanism gives an extinction prediction. The Optimized mechanism [23] is derived by optimizing the rate parameters of a 258-reaction  $C_3$  combustion mechanism that was added to a previously optimized 205-reaction  $C_{<3}$  mechanism (GRI-Mech, 1999) for a total of 463 reactions. The optimization was done with 21 optimization targets, 9 of which were ignition delays and 12 of which were atmospheric pressure laminar flame speeds [23]. The Optimized mechanism shows a good fit to unstretched propane–air flame speeds derived from stretched opposed-jet flames over a wide range of equivalence ratios ( $\phi = 0.5$  to 1.5) [30] and a good fit to propane shock tube ignition delay data. It seems to work well for most of the lean propane–air flames in this work except for this extinction case. This suggests that the use of only ignition delay and flame speed targets to validate mechanisms may be insufficient to predict flame behavior near extinction. Fig. 14 shows a near-limit flame structure:  $C_3H_8$ –air mixture ( $\phi = 0.55$ ) vs  $H_2$ –air ( $\phi = 0.28$ ) mixture ( $\kappa = 140 \text{ s}^{-1}$ ). The flame temperature is still around 1300 K. There is good agreement for tem-

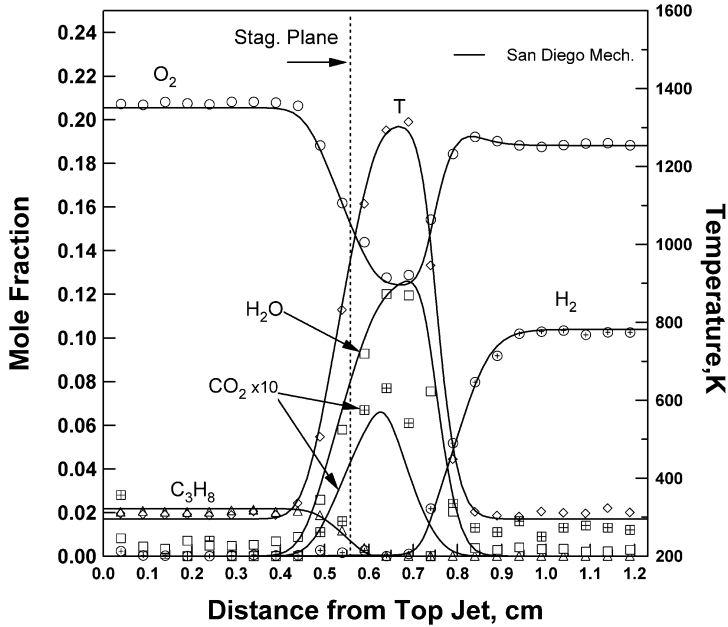


Fig. 14. Experimental and numerically predicted species and temperature profiles for a premixed opposed-jet flame:  $C_3H_8$ -air ( $\phi = 0.55$ ) vs  $H_2$ -air ( $\phi = 0.28$ ),  $\kappa = 140 \text{ s}^{-1}$ . Numerical simulation using the San Diego mechanism.

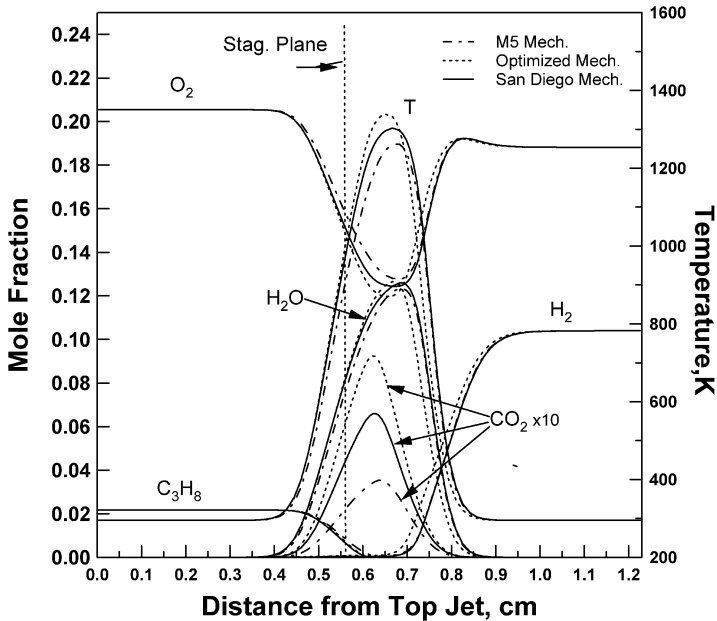


Fig. 15. Comparison of numerically predicted species and temperature profiles with three different mechanisms for a premixed opposed-jet flame:  $C_3H_8$ -air ( $\phi = 0.55$ ) vs  $H_2$ -air ( $\phi = 0.28$ ),  $\kappa = 140 \text{ s}^{-1}$ .

perature and species including carbon dioxide. The comparisons of the three mechanisms are given in Fig. 15. This mixture is very near the lean flammability limit and the three mechanisms have similar predictions, although the San Diego mechanism profiles are closest to the measurements. Since there is

only a small amount of propane diffusion across the stagnation plane leading to a small amount of  $CO_2$  (about 0.6%), the merged flame structure is hydrogen chemistry dominated and all three mechanisms give nearly the same results except for the  $CO_2$  profiles that deviate.

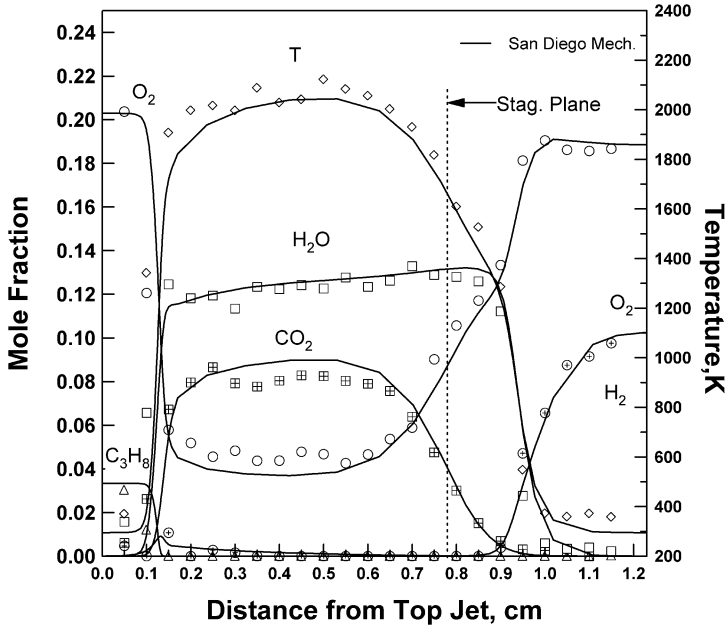


Fig. 16. Experimental and numerically predicted species and temperature profiles for a premixed opposed-jet flame:  $C_3H_8$ -air ( $\phi = 0.86$ ) vs  $H_2$ -air ( $\phi = 0.28$ ),  $\kappa = 140 \text{ s}^{-1}$ . Numerical simulation using the San Diego mechanism.

#### 4.4. Group D: Stretched strong propane-air flames

Stronger lean premixed propane-air flame structures are also studied. A premixed propane-air mixture ( $\phi = 0.86$ ) vs hydrogen-air at  $\kappa = 140 \text{ s}^{-1}$  is shown in Fig. 16. The measured peak temperature is close to 2100 K and is slightly higher than predicted. The trend for species is similar to that shown in Fig. 5. The numerical simulations in Fig. 16 are from the San Diego mechanism. The M5 and the Optimized mechanisms are used and comparisons among three mechanisms show similar trends as shown in Fig. 4. The San Diego mechanism predicts a higher flame speed (see Table 3) and gives the best predictions of the data.

Comparisons of the temperature profiles for various equivalence ratios of propane-air mixtures vs the lean hydrogen-air ( $\phi = 0.28$ ) mixture at stretch rate  $\kappa = 140 \text{ s}^{-1}$  are shown in Fig. 17. Numerical results are from the San Diego mechanism. From Fig. 17, it is found the San Diego mechanism gives a good prediction over the wide range at the stretch rate  $\kappa = 140 \text{ s}^{-1}$  except at the  $\phi = 0.66$  case. At  $\phi = 0.66$  and  $\kappa = 140 \text{ s}^{-1}$ , the San Diego mechanism predicts a stronger, self-propagating flame (see Fig. 11). This is not surprising as the San Diego mechanism predicts a higher flame speed in general (Table 3) that delays its prediction of the transition from a self-propagating premixed flame to a weak diffusion flame to a lower equivalence ratio (below  $\phi = 0.66$  at  $\kappa = 140 \text{ s}^{-1}$ ).

Fig. 17 clearly shows changes of the flame temperature and flame structure when changing the equivalence ratio. That is, equivalence ratios of 0.66 or below show the negative flame speed diffusion flame formed by interaction of the lean propane-air mixture with the lean hydrogen-air flame and its hot products when the stretch rate is fixed as  $140 \text{ s}^{-1}$ . When the mixture equivalence ratio goes above 0.66, self-propagating flames are formed and the hot products from the hydrogen-air flame have little influence.

## 5. Conclusions

Stretched laminar flame structures for a wide range of propane-air mixtures vs hot products are investigated by laser-based diagnostics and numerical simulation. The stretch effect and influence of equivalence ratio on flame structure are studied in detail.

A summary of modeling with the three mechanisms is given in Table 3. The calculated flame speed for each premixed propane-air mixture is also listed in Table 3. A positive sign indicates positive flame speed flame structure and a negative sign indicates negative flame speed flame structure. In Groups A and B, the flame structure is positive at low stretch and negative at high stretch. In Group B at  $\kappa = 140 \text{ s}^{-1}$ , the predicted flame structure is either positive flame speed flame or negative flame speed flame, depending on the chemical kinetic mechanism. All the sublimit

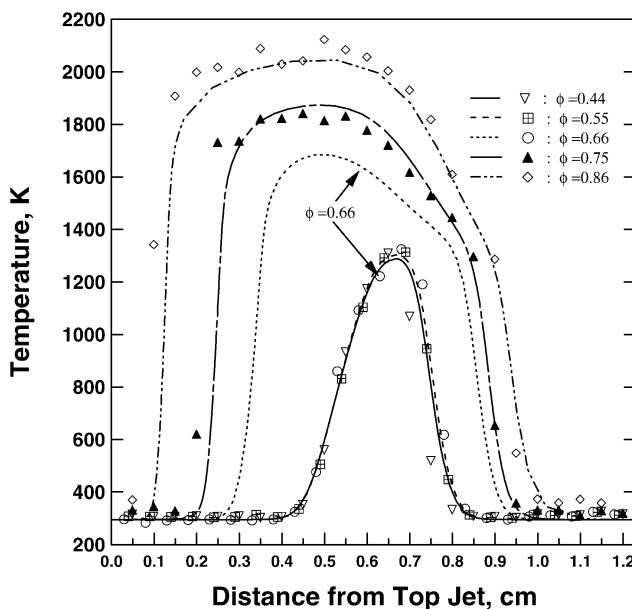


Fig. 17. Comparison of experimental and numerically predicted temperature profiles for different equivalence ratio premixed opposed-jet flames:  $C_3H_8$ -air vs  $H_2$ -air ( $\phi = 0.28$ ),  $\kappa = 140 \text{ s}^{-1}$ . Numerical simulation using the San Diego mechanism.

flames in Group C are negative flame speed flames. Group D flame structures are always positive flame speed flame for all three mechanisms.

For high-temperature self-propagating flames, the measured water vapor agrees very well with numerical predictions. Measured temperature, oxygen, and carbon dioxide slightly deviate from the predicted results. Premixed flame locations are different with each of the kinetic mechanisms and the measured flame location is closest to that predicted with the San Diego mechanism. This is expected as the San Diego mechanism was developed for high-temperature flames and it predicts the highest propane-air flame speeds (see Table 3).

For diffusion-controlled negative flame speed flames above the lean limit ( $\phi > 0.56$ ), the simulations give mixed results. The M5 mechanism sometimes predicts extinction (Table 3). When the mechanisms do properly predict a diffusion-controlled negative flame speed flame, most species concentration and temperature show very good agreement between experimental data and predicted results except for carbon dioxide (Figs. 7, 10, and 12). For example, at  $\phi = 0.66$  and  $\kappa = 140 \text{ s}^{-1}$  (Fig. 10), the predicted carbon dioxide concentration with the M5 mechanism is much lower than the experimental data, while the Optimized mechanism gives good predicted results compared to experimental data. The prediction with the San Diego mechanism gives a self-propagating flame structure at  $\kappa = 140 \text{ s}^{-1}$  (Fig. 11).

For sublimit flame structure ( $\phi = 0.44$  or  $\phi = 0.55$ ), predictions with the San Diego mechanism

are closest to experimental data even though there is some deviation for the carbon dioxide profile. For the  $\phi = 0.44$  case, the Optimized mechanism predicts extinction while the other two mechanisms give good results. For  $\phi = 0.55$  case, all three mechanisms give different predictions for carbon dioxide but the San Diego mechanism is closest to the predictions.

Overall, the San Diego mechanism gives the best prediction of these lean propane-air flames. It does fail to predict the sensitive transition from a self-propagating flame to a diffusion-controlled low-temperature flame for the conditions  $\phi = 0.66$ ,  $\kappa = 140 \text{ s}^{-1}$  and  $\phi = 0.75$ ,  $\kappa = 252 \text{ s}^{-1}$ . This can be traced to the higher flame speeds predicted by the San Diego mechanism (Table 3) that leads to a delay in the transition from a self-propagating premixed propane-air flame to a weak propane diffusion flame.

### Acknowledgments

The authors acknowledge the U.S. Department of Energy's Office of Basic Energy Sciences who has supported this work through a Partnerships for Academic-Industrial Research (PAIR) grant (No. DE-FG02-98ER14915, with Dr. Alan H. Laufer as the technical monitor).

### References

- [1] C.K. Law, Proc. Combust. Inst. 22 (1988) 1381–1402.

- [2] C.K. Law, C.J. Sung, *Prog. Energy Combust. Sci.* 26 (2000) 459–505.
- [3] M.A. Tanoff, M.D. Smooke, R.J. Osborne, T.M. Brown, R.W. Pitz, *Proc. Combust. Inst.* 26 (1996) 1121–1128.
- [4] R.S. Barlow, A.N. Karpetis, J.H. Frank, J.-Y. Chen, *Combust. Flame* 127 (2001) 2102–2118.
- [5] H.S. Xue, S.K. Aggarwal, R.J. Osborne, T.M. Brown, R.W. Pitz, *AIAA J.* 40 (2002) 1236–1238.
- [6] J.A. Wehrmeyer, Z. Cheng, D.M. Mosbacher, R.W. Pitz, R. Osborne, *Combust. Flame* 128 (2002) 232–241.
- [7] Z. Cheng, J.A. Wehrmeyer, R.W. Pitz, in: 38th AIAA/ASME/SAE/ASEE Joint Propulsion Conference, Indianapolis, IN, 2002, AIAA 2002-4021.
- [8] Z. Cheng, J.A. Wehrmeyer, R.W. Pitz, *Proc. Combust. Inst.* 30 (2005) 285–293.
- [9] M.D. Smooke, J. Crump, K. Seshadri, V. Giovangigli, *Proc. Combust. Inst.* 23 (1990) 463–470.
- [10] P.A. Libby, F.A. Williams, *Combust. Flame* 44 (1982) 287–303.
- [11] J. Buckmaster, D. Mikolaitis, *Combust. Flame* 47 (1982) 191–204.
- [12] P.A. Libby, F.A. Williams, *Combust. Sci. Technol.* 31 (1983) 1–42.
- [13] P.A. Libby, A. Liñán, F.A. Williams, *Combust. Sci. Technol.* 34 (1983) 257–293.
- [14] N. Darabiha, S.M. Candel, F.E. Marble, *Combust. Flame* 64 (1986) 203–217.
- [15] N. Darabiha, S.M. Candel, V. Giovangigli, M.D. Smooke, *Combust. Sci. Technol.* 60 (1988) 267–285.
- [16] F.A. Williams, *AGARD Conf. Proc.* 164 (1975) III-1–III-25.
- [17] S.H. Sohrab, Z.Y. Ye, C.K. Law, *Proc. Combust. Inst.* 20 (1984) 1957–1965.
- [18] D. Trees, T.M. Brown, K. Seshadri, M.D. Smooke, G. Balakrishnan, R.W. Pitz, V. Giovangigli, S.P. Nandula, *Combust. Sci. Technol.* 104 (1995) 427–439.
- [19] J.S. Kim, P.A. Libby, F.A. Williams, *Combust. Sci. Technol.* 87 (1992) 1–25.
- [20] R.J. Kee, F.M. Rupley, J.A. Miller, M.E. Coltrin, J.F. Grcar, E. Meeks, H.K. Moffat, A.E. Lutz, G. Dixon-Lewis, M.D. Smooke, J. Warnatz, G.H. Evans, R.S. Larson, R.E. Mitchell, L.R. Petzold, W.C. Reynolds, M. Caracotsios, W.E. Stewart, P. Glarorg, C. Wang, O. Adigum, W.G. Houf, C.P. Chou, S.F. Miller, *Chemkin Collection, Release 3.7, Reaction Design, Inc., San Diego, CA, 2002.*
- [21] D.C. Haworth, R.J. Blint, B. Cuenot, T.J. Poinot, *Combust. Flame* 121 (2000) 395–417.
- [22] San Diego Mechanism, <http://maeweb.ucsd.edu/~combustion/cermech>, 2003/08/30.
- [23] Z. Qin, V.V. Lissianski, H. Yang, W.C. Gardiner, S.G. Davis, H. Wang, *Proc. Combust. Inst.* 28 (2000) 1663–1669.
- [24] I. Glassman, *Combustion*, third ed., Academic Press, San Diego, CA, 1996.
- [25] H. Tsuji, I. Yamaoka, *Proc. Combust. Inst.* 19 (1982) 1533–1540.
- [26] C.J. Sung, J.B. Liu, C.K. Law, *Combust. Flame* 106 (1996) 168–183.
- [27] J. Warnatz, *Proc. Combust. Inst.* 18 (1981) 369–384.
- [28] Y. Ju, H. Guo, K. Maruta, T. Niioka, *Combust. Flame* 113 (1998) 603–614.
- [29] Y. Ju, H. Matsumi, K. Takita, G. Masuya, *Combust. Flame* 116 (1999) 580–592.
- [30] C.M. Vagelopoulos, F.N. Egolfopoulos, C.K. Law, *Proc. Combust. Inst.* 25 (1994) 1341–1347.